Oscillations of hot, young neutron stars: Gravitational wave frequencies and damping times

G. F. Burgio,[1] V. Ferrari,[2] L. Gualtieri,[2] and H.-J. Schulze[1]

[1]*INFN, Sezione di Catania, Dipartimento di Fisica, Via Santa Sofia 64, 95123 Catania, Italy*

[2]*Dipartimento di Fisica, "Sapienza" Università di Roma and Sezione INFN Roma 1, P.A. Moro 5, 00185 Roma, Italy*

(Received 14 June 2011; published 4 August 2011)

We study how the frequencies and damping times of oscillations of a newly born, hot proto-neutron star depend on the physical quantities which characterize the star quasistationary evolution which follows the bounce. Stellar configurations are modeled using a microscopic equation of state obtained within the Brueckner-Hartree-Fock, nuclear many-body approach, extended to the finite-temperature regime. We discuss the mode frequency behavior as a function of the lepton composition, and of the entropy gradients which prevail in the interior of the star. We find that, in the very early stages, gravitational wave emission efficiently competes with neutrino processes in dissipating the star mechanical energy residual of the gravitational collapse.

DOI: 10.1103/PhysRevD.84.044017 PACS numbers: 04.30.Db, 26.60.Kp, 97.10.Sj, 97.60.Jd

I. INTRODUCTION

The birth of a proto-neutron star (PNS) in a core-collapse supernova is a very difficult phenomenon to model, since it requires not only accurate descriptions of the microphysics of the collapsing matter, in particular, of neutrino transport and related processes, but also of the violent dynamical processes occurring in the contracting-exploding star, which need to be treated in the framework of general relativity (see [1] for a recent review).

The description of the subsequent PNS evolution is also challenging, because a PNS is a hot and rapidly evolving object. The physical processes which contribute to the star cooling and contraction, such as nuclear and weak interactions and energy and lepton number transport by neutrino diffusion, have to be included in dynamical simulations. Thus, most simulations of gravitational core collapse to a PNS end shortly after the core bounce and the launch of the supernova explosion—typically after a few hundreds of milliseconds—and only a few dynamical simulations extend to the first minute of the PNS life [2–5].

In this paper we are interested in this latest phase of the PNS life, when shock waves, neutrino winds, convection instabilities, and accretion flows are no longer dominant and the star cooling and contraction proceed on time scales of seconds, so that the evolution is quasistationary. In particular, we want to study how the frequencies and damping times of the PNS quasinormal modes of oscillation depend on the internal structure of the star. The main motivation is that the oscillations of a newly born PNS may be associated to gravitational wave signals with sizeable amplitudes, and with frequencies lower than those typical of mature neutron stars. This would favor their detection by the next generation of ground-based interferometers LIGO/Virgo and their future version, the Einstein Telescope [6–8].

The available dynamical simulations of the post-bounce evolution of a PNS indicate that, typically, the star goes through the following main steps. After the core bounce, a shock wave propagates through the outer PNS mantle, leaving behind a low-entropy core in which neutrinos are trapped, surrounded by a low-density, high-entropy envelope. The mantle accretes matter from the outer layers and rapidly contracts, losing energy due to electron captures and thermal neutrino emission. The supernova explosion lifts off the stellar envelope and, in a few tenths of seconds, due to extensive neutrino losses, the lepton pressure decreases and the envelope contracts. At this stage the PNS radius is about 20–30 km; the subsequent evolution can be described as a sequence of equilibrium configurations; this quasistationary evolution is the phase of interest for us.

Simulations show that the diffusion of high-energy neutrinos (of the order of a few hundred MeV) from the low-entropy core to the high-entropy envelope, from which they finally escape with energies of the order of a few tens of MeV, generates a large amount of heat within the star, producing temperatures up to several tens of MeV; as a result, the core entropy approximately doubles, whereas the entropy of the envelope decreases. In a few tens of seconds the PNS becomes lepton poor, but it is still hot. The net number of neutrinos in the interior is low, but thermally produced neutrino pairs of all flavors are abundant, and dominate the emission; the star cools down and entropy gradients are gradually smoothed out, while the average neutrino energy decreases, and neutrinos mean free path increases; after approximately one minute it becomes comparable to the stellar radius, and the star becomes neutrino transparent. By this time, the temperature has dropped to 1–5 MeV (≈ 1–5×10^{10} K) and the star has radiated off almost all of its binding energy, becoming what we call a neutron star (NS).

This brief summary of the first minute of the PNS life is deliberately imprecise, because the details of the evolution depend on the assumptions on which the simulation is based. For instance, in [2–4], where the first minute after the core bounce is considered, the evolution is treated as a

 © 2011 American Physical Society

sequence of quasistationary states: the thermodynamical variables and the lepton fractions are determined by solving evolution equations (for instance Boltzmann's equation to model neutrino transport), whereas at each time step the stellar structure is found by solving the Tolman-Oppenheimer-Volkov equations. In [5], instead, all quantities are determined through a time-evolution core-collapse code, which has been extended in order to describe the first $\sim$20 s of the post-bounce processes. However, there are features which are common to different studies; indeed, starting from an initial configuration characterized by a low-entropy core and a high-entropy envelope, due to neutrino processes the star goes smoothly through the following phases:

(i) the entropy increases in the core while decreasing in the envelope;
(ii) entropy gradients gradually smooth out while the star is still hot;
(iii) the star progressively cools down, and the overall entropy decreases;
(iv) the evolution ends in the ''cold'', zero entropy, neutron star configuration.

We remark that both in [2–4] and in [5] the equation of state (EOS) of baryonic matter is a finite-temperature, field-theoretical model solved at the mean-field level.

In this paper, instead, we employ a microscopic EOS obtained within the Brueckner-Hartree-Fock (BHF) nuclear many-body approach extended to the finite-temperature regime, as we shall discuss in Sec. III. Our aim is to explore how the frequencies and damping times of the PNS quasinormal modes depend on the physical quantities which characterize the quasistationary configurations, which are essentially the entropy profile (which will appear to be the most important in this respect) and the lepton composition. Furthermore, we want to model different stages of a possible evolutive sequence of stationary configurations.

PNSs are expected to be rapidly rotating; in our study we neglect rotation, since we are primarily interested in the effects of the thermal and chemical evolution on the star oscillation frequencies, and in comparing the results with those of previous works which use different EOSs to model the PNS. We do not expect these effects to change significantly in a rotating star. However, it should be mentioned that quasinormal mode frequencies are affected by the star rotation [9–11]: the degeneracy in the harmonic index m is removed, and modes with $m > 0$ have frequencies lower than those of a nonrotating star. This enhances detection chances, since ground-based inteferometers are more sensitive at lower frequencies.

The article is organized as follows. In Sec. II we briefly explain how to compute the complex values of the quasinormal mode frequencies using the relativistic theory of stellar perturbations. In Sec. III the derivation of the equation of state of hot nuclear matter used to model the PNS evolution is shortly illustrated. In Sec. IV we discuss how the different stages of a PNS quasistationary evolution are simulated by constructing stellar configurations with appropriate entropy and lepton fraction profiles. In Sec. V we compute and discuss the stellar parameters and the quasinormal mode frequencies for the various configurations. Conclusions are drawn in Sec. VI.

II. THE QUASINORMAL MODES OF NEUTRON STARS

A. Stellar perturbations

In order to find frequencies and damping times of the quasinormal modes (QNMs) of a star, we need to solve the equations describing nonradial perturbations of a (spherically symmetric) star in general relativity, which we briefly recall.

The perturbed spacetime metric is expanded in tensor spherical harmonics, as (we use geometrized units, assuming $c = G = 1$)

$$\begin{aligned} ds^2 = & -e^{\psi}(1 + r^{\ell} H_0^{\ell m} Y_{\ell m} e^{i\omega t}) dt^2 \\ & + e^{\lambda}(1 - r^{\ell} H_2^{\ell m} Y_{\ell m} e^{i\omega t}) dr^2 \\ & - 2i\omega r^{\ell+1} H_1^{\ell m} Y_{\ell m} e^{i\omega t} dt dr \\ & + r^2(1 - r^{\ell} K^{\ell m} Y_{\ell m} e^{i\omega t})(d\vartheta^2 + \sin^2\theta d\varphi^2), \end{aligned} \tag{1}$$

where ω is the frequency, $Y_{\ell m}(\vartheta, \varphi)$ are the scalar spherical harmonics, and $H_i^{\ell m}(r)$, $K^{\ell m}(r)$ describe the metric perturbations with polar parity, i.e., those transforming as $(-1)^{\ell}$ under a parity transformation. In this paper we do not consider perturbations with axial parity, which transform as $(-1)^{\ell+1}$. The functions $\psi(r)$, $\lambda(r)$ describe the unperturbed metric, and are found by solving the Tolman-Oppenheimer-Volkov equations. The four-velocity of the generic fluid element is

$$\begin{aligned} u^{\mu} &= u_0^{\mu} + \delta u^{\mu} \\ &= (e^{-\psi/2}, 0, 0, 0) + i\omega e^{-\psi/2}(0, \xi^r, \xi^{\theta}, \xi^{\phi}), \end{aligned} \tag{2}$$

where ξ_{μ} is the fluid element Lagrangian displacement, expanded in vector spherical harmonics

$$\begin{aligned} \xi_r(t, r, \vartheta, \varphi) &= e^{\lambda/2} r^{\ell-1} W^{\ell m}(r) Y_{\ell m}(\vartheta, \varphi) e^{i\omega t}, \\ \xi_{\vartheta}(t, r, \vartheta, \varphi) &= -r^{\ell} V^{\ell m}(r) \partial_{\vartheta} Y_{\ell m}(\vartheta, \varphi) e^{i\omega t}, \\ \xi_{\varphi}(t, r, \vartheta, \varphi) &= -r^{\ell} V^{\ell m}(r) \partial_{\varphi} Y_{\ell m}(\vartheta, \varphi) e^{i\omega t}. \end{aligned} \tag{3}$$

The fluid is also characterized by its pressure and energy density

$$\begin{aligned} p(r) + \delta p(t, r, \vartheta, \varphi) &= p(r) + r^{\ell} \delta p^{\ell m}(r) Y_{\ell m}(\vartheta, \varphi) e^{i\omega t}, \\ \varepsilon(r) + \delta\varepsilon(t, r, \vartheta, \varphi) &= \varepsilon(r) + r^{\ell} \delta\varepsilon^{\ell m}(r) Y_{\ell m}(\vartheta, \varphi) e^{i\omega t}. \end{aligned} \tag{4}$$

We denote with δ the Eulerian perturbations, and with Δ the Lagrangian perturbations, so that for instance the Lagrangian perturbation of the pressure is

$$\Delta p = \delta p + \xi^r \frac{\partial p}{\partial r}, \tag{5}$$

i.e.,

$$\Delta p^{\ell m} = \delta p^{\ell m} + \frac{e^{-\lambda/2}}{r} W^{\ell m} \frac{\partial p}{\partial r}. \tag{6}$$

Einstein's equations, linearized in the perturbations, yield a system of ordinary differential equations for the perturbed functions. Different equivalent sets of equations have been derived in the literature, using different gauge choices or different combinations of the relevant equations [12–15]. In this paper we use the formulation of Lindblom and Detweiler [13,14], consisting of a system of four first-order differential equations for the functions $\{H_1^{\ell m}, K^{\ell m}, W^{\ell m}, X^{\ell m}\}$, where

$$X^{\ell m} = -e^{\psi/2} \Delta p^{\ell m}, \tag{7}$$

and algebraic relations which allow to compute the remaining functions $\{H_0^{\ell m}, H_2^{\ell m}, V^{\ell m}\}$ in terms of the others (see Appendix A). To close the system, an EOS, relating the energy density ε and the pressure p, has to be assigned.

B. The quasinormal mode frequencies

A QNM is a solution of the perturbation equations, which is regular at the center, continuous on the surface, and which behaves as a pure outgoing wave at infinity. Since in general relativity a nonradial oscillation is associated with gravitational wave (GW) emission, such solutions belong to complex frequencies:

$$\omega = \sigma + \frac{\mathrm{i}}{\tau_{\mathrm{GW}}}, \tag{8}$$

where $\sigma = 2\pi\nu$ and ν is the pulsation frequency; τ_{GW} is the damping time of the mode due to gravitational wave emission. If the mode is unstable, its imaginary part is negative and $-\tau_{\mathrm{GW}}$ is the growth time of the instability.

The procedure to find the QNM frequencies is the following: (i) We choose a value of l and a complex value of ω (since the background is spherical, the equations do not depend on the index m). (ii) We integrate Eqs. (A1), by imposing that the solution is regular at the center and that $\Delta p = 0$ at the stellar surface [Eqs. (A3) and (A4)]. (iii) We impose that the solution and its first derivative are continuous on the stellar surface, and find the metric perturbations outside the star. (iv) In vacuum, the perturbed equations reduce to a simple, second-order differential equation (the Zerilli equation (A6)), which we integrate up to radial infinity. (v) We check whether the solution satisfies the outgoing wave boundary condition at infinity (A8) which identifies a quasinormal mode; we then repeat the procedure for different values of ω. The values of ω which satisfy the outgoing wave condition can be found using a Newton-Raphson method.

The polar QNMs are classified, following a scheme introduced by T. G. Cowling in Newtonian theory [16], on the basis of the restoring force which prevails when the generic fluid element is displaced from the equilibrium position. Thus, we have a g-mode if the restoring force is mainly provided by buoyancy or a p-mode if it is due to a pressure gradient. The frequencies of the g-modes are lower than those of the p-modes, and the two sets are separated by the frequency of the fundamental (f-) mode, which is related to a global oscillation of the fluid. In general relativity there exist further modes, named w-modes [17], that are purely gravitational, since they barely excite the fluid motion. Other classes of modes are associated to NS features which are not included in the present model, like rotation, magnetic fields, the crust rigidity.

C. Sound speed

A neutron star at the end of its evolution is cold and isentropic, matter is in beta-equilibrium and can be described by a barotropic EOS $p = p(\varepsilon)$. Conversely, when the star is young and hot the EOS cannot be expressed in a barotropic form, since the pressure depends nontrivially on the entropy and on the composition, i.e.,

$$p = p(\varepsilon, s, x_i). \tag{9}$$

Therefore, to solve the perturbed equations the profiles of entropy and particle fractions, respectively $s(n)$ and $x_i(n)$, are also needed. In Eq. (9) n is the baryon number density, $s = S/A$ is the entropy per baryon, and $x_i = n_i/n$ is the fraction of the ith particle. Usually matter is locally in beta equilibrium and neutrinos are trapped, therefore the dependence on the composition $\{x_i\}$ reduces to a dependence on the lepton fraction $Y_e = x_e + x_{\nu_e}$ only.

The perturbed equations (A1) depend explicitly on the sound speed c_s^2, which relates the Lagrangian perturbations of pressure and energy density,

$$\Delta p = c_s^2 \Delta \varepsilon. \tag{10}$$

c_s^2 is defined as the following thermodynamical derivative

$$c_s^2 = \left(\frac{\partial p}{\partial \varepsilon}\right)_{\mathrm{adiabatic}}, \tag{11}$$

where "adiabatic" means that the derivative is performed keeping fixed the entropy and the fractions of those particle species *which do not change during the pulsation* [18].

To clarify this statement, let us consider a fluid element oscillating with period t_{osc} about the equilibrium position. The following equation holds:

$$\Delta p = \left(\frac{\partial p}{\partial \varepsilon}\right)_{s,x_i} \Delta \varepsilon + \left(\frac{\partial p}{\partial s}\right)_{\varepsilon,x_i} \Delta s + \sum_i \left(\frac{\partial p}{\partial x_i}\right)_{\varepsilon,s} \Delta x_i. \tag{12}$$

Since we are considering adiabatic perturbations, the fluid element does not exchange heat with its surroundings and $\Delta s = 0$. Furthermore, the displaced fluid element has

a composition different from the surrounding fluid even though nuclear reactions, acting on a time scale $t_{\rm react}$, tend to eliminate this difference. The two limiting cases are:

(i) $t_{\rm react} \gg t_{\rm osc}$; in this case the fluid element composition does not change during the oscillation, i.e., $\Delta x_i = 0$, and by combining Eqs. (10) and (12) we find

$$c_s^2 = \left(\frac{\partial p}{\partial \varepsilon}\right)_{s,x_i}. \tag{13}$$

(ii) $t_{\rm react} \ll t_{\rm osc}$; the fluid element composition changes, becoming that of the surrounding fluid. By replacing the composition profile $x_i = x_i(\varepsilon, s, Y_e)$ in (9), it is possible to express the EOS as $p = p(\varepsilon, s, Y_e)$. Equations (10) and (12) then give

$$c_s^2 = \left(\frac{\partial p}{\partial \varepsilon}\right)_{s,Y_e}. \tag{14}$$

for beta-stable, neutrino-trapped matter.

For the PNSs in quasistationary evolution we consider in this paper, typical oscillation periods are of the order $t_{\rm osc} \approx 10^{-3}$ s, while weak interaction time scales are [19]

$$t_{\rm react}^{(1)} \approx \frac{5 \times 10^6 \text{ s}}{(T/10^9 \text{ K})^6}, \qquad t_{\rm react}^{(2)} \approx \frac{20 \text{ s}}{(T/10^9 \text{ K})^4} \tag{15}$$

for modified and direct Urca processes, respectively. In the first seconds of a PNS life $T \approx (1\text{–}4) \times 10^{11}$ K, thus $t_{\rm react}^{(1,2)} \ll t_{\rm osc}$. Therefore the stellar pulsations always occur in local beta equilibrium. Time scales of strong nuclear reactions are even smaller.

D. Some considerations on the f- and g-modes

For old, cold neutron stars, the frequency of the f-mode, ν_f, is in the range 1–3 kHz, and the damping time, τ_f, is of the order of a few tenths of seconds. According to the Newtonian theory of stellar pulsations, ν_f scales as the square root of the star average density, and this behavior is maintained in the relativistic theory, according to which the damping time scales as $\tau_f \sim R^4/M^3$ [20–22].

The g-modes are directly related to the thermodynamical properties of the star. Indeed, their presence can be traced back to the Schwarzschild discriminant [23],

$$S(r) = \frac{dp}{dr} - c_s^2 \frac{d\varepsilon}{dr} = \frac{dp}{dr}\left(1 - \frac{c_s^2}{c_{s0}^2}\right), \tag{16}$$

where $c_{s0}^2 = \frac{dp/dr}{d\varepsilon/dr}$. The radial acceleration of a fluid element displaced from equilibrium by Δr is

$$a = -\frac{e^{-\lambda/2}}{(\varepsilon + p)^2 c_s^2} \left|\frac{dp}{dr}\right| S(r)\Delta r. \tag{17}$$

Therefore, if $S(r) > 0$ the fluid element oscillates about the equilibrium position, whereas if $S(r) < 0$ it is accelerated away from equilibrium. It follows that, if in some region of the star $S(r) < 0$, this region is convectively unstable and the star admits a set of unstable g-modes, otherwise the g-modes are stable. If $S(r)$ vanishes identically, the star does not have g-modes (all g-modes degenerate to zero frequency). This is the case if the neutron star is cold and old, since the EOS is barotropic and $c_s^2 = \frac{p_{,r}}{\varepsilon_{,r}}$. Similar information is contained in the Brunt-Väisälä frequency which, in a relativistic framework, is defined as [24]

$$N^2(r) = \frac{e^{\psi - \lambda}}{(\varepsilon + p)c_s^2} \frac{\psi_{,r}}{2} S(r). \tag{18}$$

It has been shown that, although the Brunt-Väisälä frequency changes by many orders of magnitude throughout the star, it allows to estimate some g-mode frequencies of Newtonian stars. For instance, in [25] the frequency of higher-order g-modes of main sequence stars is computed using the following formula

$$\sigma_g \approx \frac{\sqrt{\ell(\ell+1)}}{(2\kappa + \ell + n_e + \frac{1}{2})\frac{\pi}{2}} \int_0^R dr \frac{|N(r)|}{r}, \tag{19}$$

where R is the stellar radius, κ is the order of the g-mode, and n_e is the effective polytropic index of the outer layers of the star. However, the Brunt-Väisälä frequency cannot be used to estimate neutron star g-mode frequencies [24]; these frequencies can only be found by solving the perturbation equations, as we do in the present paper. Nevertheless the following considerations will be useful to interpret the results we will show in the following. Equation (19) indicates that higher frequency values correspond to larger values of $S(r)$ (i.e., of $|N(r)|$) inside the star. Since we shall assume $dY_e/dr = 0$ (see Sec. IV), we have

$$S(r) = \frac{dp}{dr} - \left(\frac{\partial p}{\partial \varepsilon}\right)_{s,Y_e} \frac{d\varepsilon}{dr} = \left(\frac{\partial p}{\partial s}\right)_{\varepsilon,Y_e} \frac{ds}{dr}, \tag{20}$$

we may expect that higher g-mode frequencies correspond to larger entropy gradients.

E. The damping time of quasinormal modes

A QNM of a PNS is characterized by the pulsation frequency and by the damping time $\tau_{\rm GW}$. Its value is important because it shows how fast the pulsation energy can be dissipated through gravitational wave emission, and it must be compared to the time scale $\tau_{\rm diss}$ associated with other dissipative processes which may compete with GW emission. These include viscosity, heat transport, neutrino diffusion, etc. (phenomena which we are neglecting in our model). In the first minute of life of a PNS, $\tau_{\rm diss} \sim$ 10–20 s [26,27] (see also the discussion in [6]). Thus, if $\tau_{\rm GW} \ll \tau_{\rm diss}$, the oscillations are mainly damped by gravitational wave emission, and vice versa. We also remark that, if a QNM is unstable, the instability can grow only if $\tau_{\rm GW} \ll \tau_{\rm diss}$.

As long as $\tau_{\rm GW} \ll \tau_{\rm diss}$, when a star oscillates in a QNM, the pulsation energy changes in time as [12]

$$E_{\rm puls}(t) \approx E_{\rm puls}(0) e^{-2t/\tau_{\rm GW}}, \tag{21}$$

and the power radiated in gravitational waves is

$$L_{\rm GW} = -\dot{E}_{\rm puls} \approx 2E_{\rm puls}/\tau_{\rm GW}. \tag{22}$$

Thus, smaller QNM damping times are associated with a more efficient gravitational wave emission. In the case of cold NSs, the f-mode has always the smallest damping time, but this is not always the case for PNSs, as we shall discuss later.

Although we shall compute the damping times of all modes by direct integration of the perturbed equations, it is useful to give some approximate formula which will allow us to explain some results of the next sections. From Eq. (22) we find

$$\tau_{\rm GW} \approx 2E_{\rm puls}/L_{\rm GW}. \tag{23}$$

The (approximate) expressions of $E_{\rm puls}$ and $L_{\rm GW}$ (the latter is obtained using the quadrupole formalism) can be found in [24,28] and are, in terms of the perturbation functions defined in this paper,

$$E_{\rm puls} \approx \frac{1}{2}\sigma^2 \int_0^R dr r^{2\ell}(\varepsilon + p) e^{(\lambda-\psi)/2}[|W^{\ell m}|^2 + \ell(\ell+1)|V^{\ell m}|^2] \tag{24}$$

and

$$L_{\rm GW} \approx \frac{4\pi}{75}\sigma^6 \left| \int_0^R dr r^4 \delta\varepsilon^{\ell m} \right|^2, \tag{25}$$

where

$$\delta\varepsilon^{\ell m} = -r^\ell \left[\frac{e^{-\psi/2}}{c_s^2} X^{\ell m} + \varepsilon_{,r} \frac{e^{-\lambda/2}}{r} W^{\ell m} \right]. \tag{26}$$

III. THE EQUATION OF STATE OF HOT NUCLEAR MATTER

A. BHF many-body approach

One of the most advanced microscopic approaches to the EOS of nuclear matter is the Brueckner theory [29], recently extended to the finite-temperature regime within the Bloch-De Dominicis formalism [30]. In this approach, the essential ingredient is the two-body scattering matrix K, which, along with the single-particle potential U, satisfies the self-consistent equations

$$\langle 12|K(W)|34\rangle = \langle 12|V|34\rangle + {\rm Re}\sum_{3',4'} \langle 12|V|3'4'\rangle \times \frac{[1-n^F(3')][1-n^F(4')]}{W - E_{3'} - E_{4'} + i\varepsilon} \times \langle 3'4'|K(W)|34\rangle \tag{27}$$

and

$$U(1) = \sum_2 n^F(2)\langle 12|K(W)|12\rangle_A, \tag{28}$$

where $1, 2, \ldots$ generally denote momentum, spin, and isospin. Here V is the two-body interaction, $W = E_1 + E_2$ represents the starting energy, and $E_i = k_i^2/2m_i + U(k_i)$ the single-particle energy; $n^F(k)$ is the Fermi distribution at finite temperature. For assigned partial densities and temperature, Eqs. (27) and (28) have to be solved self-consistently along with the following equations for the auxiliary chemical potentials $\tilde{\mu}_i$,

$$n_i = \sum_k n_i^F(k) = \sum_k \frac{1}{e^{\beta(E_i(k)-\tilde{\mu}_i)}+1}, \tag{29}$$

and the baryon number density is $n = \sum_i n_i$.

At finite temperature the EOS, and all thermodynamical quantities, can be obtained from the grand-canonical potential density ω. In the Bloch-De Dominicis approach, ω can be written as the sum of a mean-field term and a correlation contribution [29,31],

$$\omega = -\sum_k \left[\frac{1}{\beta} \ln(1 + e^{-\beta(E_k - \tilde{\mu})}) + n^F(k)U(k) \right] + \frac{1}{2}\sum_k n^F(k)U(k). \tag{30}$$

In this framework, the free energy density is

$$f = \omega + n\tilde{\mu}, \tag{31}$$

and all remaining thermodynamical quantities of interest, namely, the "true" chemical potential μ, pressure p, entropy per baryon s, and energy density ε can be computed from it as

$$\mu = \frac{\partial f}{\partial n}, \tag{32}$$

$$p = n^2 \frac{\partial (f/n)}{\partial n} = \mu n - f, \tag{33}$$

$$s = -\frac{1}{n}\frac{\partial f}{\partial T}, \tag{34}$$

$$\varepsilon = f + Tns + m_n n \tag{35}$$

(m_n neutron mass). Since at zero temperature the nonrelativistic microscopic approaches do not correctly reproduce the nuclear matter saturation point, $n_0 \approx 0.17$ fm^{-3}, $E/A \approx -16$ MeV, three-body forces (TBF) among nucleons are usually introduced in order to correct this deficiency. Given the current lack of a complete microscopic theory of TBF, we have adopted the phenomenological Urbana model [32], which consists of an attractive term due to two-pion exchange with excitation of an intermediate Δ resonance and a repulsive phenomenological central

term. For simplicity, we reduce the TBF to a density-dependent two-body force by averaging over the position of the third particle, assuming that the probability of having two particles at a given distance is reduced according to the two-body correlation function. The corresponding EOS at zero temperature reproduces the nuclear matter saturation point correctly [33–35], and fulfills several requirements from the nuclear phenomenology. In all calculations presented in this paper we use the Argonne V_{18} nucleon-nucleon potential [36] together with the phenomenological Urbana TBF.

Results for symmetric nuclear matter and purely neutron matter have been obtained for different values of the temperature, and are discussed in [37–40]. In particular, in Ref. [39] useful numerical parametrizations of the EOS are given that are employed in the current work.

The Brueckner approach provides a realistic modeling of nuclear matter only at densities above about half normal nuclear matter density. Below this threshold, clustering sets in, and the system becomes inhomogeneous. Therefore, in this "low-density" regime another theoretical approach has to be used, and we employ the EOS of Shen [41], which is essentially a liquid-drop-type model at finite temperature.

Of course, since two different theoretical descriptions of the same state of matter are involved, the joining of the two EOSs requires the thermodynamical observables to be continuous functions of the baryon density. In practice we perform a Maxwell construction by equating pressure and chemical potentials of the low- and high-density sectors, and verify that the other thermodynamic variables do not exhibit significant discontinuities at the transition point. In this way, a very wide range of baryon density is spanned, from the iron density at the surface up to 8–10 times the nuclear saturation density in the core. Further details are discussed in the following subsection.

B. Composition and EOS of hot stellar matter

In neutrino-trapped β-stable nuclear matter, the chemical potential of any particle $i = n, p, l$ is uniquely determined by the conserved quantities, baryon number B_i, electric charge Q_i, and weak charges (lepton numbers) $L_i^{(e)}$, $L_i^{(\mu)}$:

$$\mu_i = B_i\mu_n - Q_i(\mu_n - \mu_p) + L_i^{(e)}\mu_{\nu_e} + L_i^{(\mu)}\mu_{\nu_\mu}. \quad (36)$$

For stellar matter containing nucleons and leptons as relevant degrees of freedom, the chemical equilibrium conditions read explicitly as

$$\mu_n - \mu_p = \mu_e - \mu_{\nu_e} = \mu_\mu + \mu_{\bar{\nu}_\mu}. \quad (37)$$

At given baryon number density n, these equations have to be solved together with the charge neutrality condition

$$\sum_i Q_i x_i = 0, \quad (38)$$

and those expressing conservation of lepton numbers

$$Y_l = x_l - x_{\bar{l}} + x_{\nu_l} - x_{\bar{\nu}_l}, \qquad l = e, \mu. \quad (39)$$

When neutrinos have left the system, their partial densities and chemical potentials vanish and the above equations simplify accordingly. We fix the muon fractions to $Y_\mu = 0$, and let Y_e assume a finite value different from zero in neutrino-trapped matter.

The nucleon chemical potentials are obtained from the free energy density f, Eq. (31),

$$\mu_i(\{n_j\}) = \frac{\partial f}{\partial n_i}\bigg|_{n_{j\neq i}}, \qquad i = n, p, \quad (40)$$

and the chemical potentials of the noninteracting leptons are obtained by solving numerically the free Fermi gas model at finite temperature. Once the hadronic and leptonic chemical potentials are known, one can proceed to calculate the composition of the β-stable stellar matter, and then the total pressure p through the usual thermodynamical relation

$$p = n^2\frac{\partial(f/n)}{\partial n} = \sum_i \mu_i n_i - f. \quad (41)$$

An important feature of the low-density domain is the treatment of neutrino trapping. Physically, neutrinos escape rapidly from the low-density matter during the PNS evolution, and the lepton number is not conserved anymore. This effect can be roughly modeled by introducing a neutrino sphere inside which neutrinos are trapped. Typical model-dependent values for the location of the neutrino sphere found in the literature are 2×10^{-3} fm^{-3} [42], 6×10^{-4} fm^{-3} [43], and 2×10^{-5} fm^{-3} [44]. Given these variations, we choose the following "natural cutoff" procedure: when imposing a constant Y_e at any density, at a certain threshold number density $n_\nu \approx 10^{-5}$–10^{-6} fm^{-3}, the electron fraction x_e becomes equal to Y_e, and neutrinos disappear naturally. For lower densities we consider the matter untrapped. This simple procedure avoids making assumptions about the neutrino sphere, although a more satisfactory treatment of neutrino trapping is required; but this is beyond the main goal of the present paper.

IV. PROTO-NEUTRON STAR STELLAR MODELS: ENTROPY AND LEPTON FRACTION PROFILES

We shall now construct equilibrium stellar models, all with a fixed baryonic mass $M_B = 1.5M_\odot$ (a conserved quantity during the stellar evolution), and with different entropy and composition profiles. These configurations will be used to simulate the quasistationary evolution of a PNS, and to compute how the stellar parameters and the quasinormal mode frequencies change during the evolution. As discussed in the introduction, the quasistationary evolution typically starts with configurations characterized by a low entropy per baryon in the core (order of $s \sim 1$ at

the center, see for instance [2]) and a large entropy per baryon in the envelope (order of $s \sim 5$ or larger). Thus, we shall consider as "initial" the configuration with an entropy per baryon profile made of two constant pieces, $s_c = 1$ in the core and $s_e = 5$ in the envelope, with a smooth junction between them. Furthermore, as discussed in Sec. III B, to model neutrino trapping we shall assume that the lepton fraction Y_e is constant throughout the star (up to a threshold density, below which $Y_e = x_e$).

As long as the evolution proceeds, entropy gradients are gradually smoothed out: the core entropy increases, the envelope entropy decreases, neutrinos escape from the surface and the star progressively cools down. To model this evolution, we construct EOSs and stellar configurations corresponding to increasing values of s_c, decreasing values of s_e and a decreasing lepton fraction; then, to decreasing values of both s_c, s_e, and a decreasing lepton fraction. Each configuration depends on the three constants s_c, s_e, Y_e, and it is labeled by P_{s_c,s_e,Y_e}.

To describe the latest stages of the PNS evolution we also consider two constant entropy profiles: (i) one with $s_c = s_e = 1$ and no neutrino trapping, $P_{1,1,x_\nu=0}$, with Y_e varying from 0.10 at the center to 0.44 at the stellar surface; (ii) a zero-temperature profile with no neutrino trapping, $P_{T=0}$, which describes a cold, old NS, with electron fraction varying from 0.09 at the center to 0.44 at the surface.

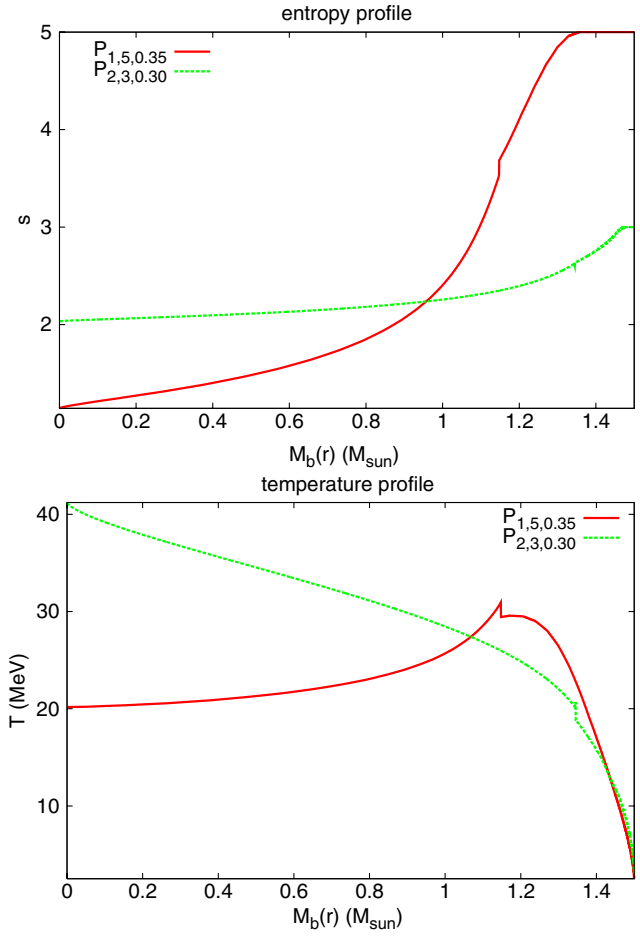

FIG. 1 (color online). The profiles of entropy (upper panel) and temperature (lower panel) are plotted versus the enclosed baryonic mass for the models $P_{1,5,0.35}$ ($R = 30.3$ km) and $P_{2,3,0.30}$ ($R = 16.5$ km).

TABLE I. Stellar models with fixed baryonic mass $M_B = 1.5M_\odot$ corresponding to different entropy profiles and lepton fractions. The gravitational mass M, radius R, central temperature T^c, and central neutrino fraction x_ν^c are tabulated for each profile.

s_c	s_e	Y_e	$M/M_\odot$	R (km)	T^c (MeV)	x_ν^c
1.0	5.0	0.38	1.43	31.5	19.8	0.052
1.0	5.0	0.35	1.43	30.3	20.2	0.041
1.0	5.0	0.28	1.42	29.4	21.2	0.020
1.5	4.5	0.33	1.43	24.6	30.3	0.035
1.5	4.5	0.32	1.42	24.4	30.5	0.031
2.0	4.0	0.32	1.43	21.5	40.5	0.033
2.0	4.0	0.30	1.43	21.3	41.0	0.027
2.0	3.0	0.30	1.42	16.5	41.2	0.026
2.0	3.0	0.28	1.41	16.4	41.8	0.021
2.0	2.0	0.28	1.41	14.5	41.6	0.020
2.0	2.0	0.23	1.40	14.1	42.9	0.010
1.0	1.0	0.23	1.37	12.5	20.2	0.007
1	1	$x_\nu = 0$	1.36	12.2	20.9	0.000
	$T = 0$		1.35	11.9	0.00	0.000

We show in Fig. 1 the profiles of the entropy per baryon (upper panel) and of the temperature (lower panel) as a function of the enclosed baryonic mass, for the models $P_{1,5,0.35}$ (radius $R = 30.3$ km) and $P_{2,3,0.30}$ (radius $R = 16.5$ km). In order to avoid sharp transitions from the core to the envelope region, we adopt a cubic interpolation for the entropy between the two regions. Thus, the entropy is a continuous function of the density. However, as a consequence of the Maxwell construction used to join the Shen EOS (low-density region) to the BHF EOS (high-density region), as discussed in the previous section, there is a weak discontinuity both in the entropy and in the temperature profile, when plotted as a function of the enclosed mass as in Fig. 1. We have checked that the results presented in the next section are not influenced by these discontinuities.

In Table I we show the quantities which characterize the stellar models associated to different profiles, namely, gravitational mass, stellar radius, temperature and neutrino fraction at the center of the star. The dependence of the stellar parameters on the temperature and lepton fraction profiles will be discussed in the next section.

V. RESULTS

In this section we discuss the behavior of the stellar radius and of frequencies and damping times of the QNMs computed for stellar models with different entropy profiles and lepton/neutrino fraction content, in order to

TABLE II. Frequencies (in Hz) and damping times (in s) of the QNMs g_1, f, p_1 for different stellar models with baryonic mass $1.5M_\odot$, lepton fraction $Y_e = 0.32$, and different entropy profiles. The central temperature T^c (in MeV) and the stellar radius R (in km) are also shown.

s_c	s_e	Δs	T^c	R	ν_{g_1}	τ_{g_1}	ν_f	τ_f	ν_{p_1}	τ_{p_1}
1.0	5.0	4	20.6	29.6	906	6.27	1194	4.42	1528	0.75
1.5	4.5	3	30.5	24.3	910	42.9	1346	0.76	1845	0.55
1.0	4.0	3	20.2	18.4	870	793	1741	0.27	2574	0.99
2.0	4.0	2	40.5	21.5	669	2×10^3	1449	0.45	2097	0.72
2.0	3.0	1	40.7	16.8	492	6×10^5	1714	0.25	2977	1.64

understand how these quantities are affected by the PNS internal structure.

Let us consider the dependence on the entropy profile first, and fix the value of the lepton fraction to $Y_e = 0.32$. We compute and compare the mode frequencies and damping times of the following stellar configurations: $P_{1,5,0.32}$, $P_{1,4,0.32}$, $P_{1.5,4.5,0.32}$, $P_{2,4,0.32}$, and $P_{2,3,0.32}$. The core-envelope "entropy jumps" are $\Delta s = 4, 3, 3, 2, 1$, respectively. In Table II we show for each profile the central temperature, the radius, and the frequencies and damping times of the QNMs g_1, f, p_1. These data allow us to discuss how the different quantities change with the entropy profile.

As a general rule, the radius is larger if the star is hotter, or equivalently, if it has a larger entropy per baryon. This is indeed confirmed comparing, for example, the profiles $P_{1,5,0.32}$ and $P_{1,4,0.32}$. The temperature (entropy) at the center is the same, but the first model has larger entropy and temperature in the envelope; its radius, $R = 29.6$ km, is larger than that of the second model, $R = 18.4$ km. This behavior is confirmed by comparing $P_{2,4,0.32}$ and $P_{2,3,0.32}$. In a similar way, the radius depends on the entropy in the core, although the dependence is weaker, because the envelope has more freedom to expand than the core; for instance, the configuration $P_{2,4,0.32}$ has a radius $R = 21.5$ km, larger than $R = 18.4$ km of $P_{1,4,0.32}$.

As discussed in Section II D, the frequency of the first g-mode depends mainly on the core-envelope entropy jump: higher values of $\Delta s = s_e - s_c$ correspond to larger g-mode frequencies. Furthermore, as argued in [45], the g-mode frequency has also a (weaker) dependence on the central temperature; indeed, the configurations $P_{1.5,4.5,0.32}$ and $P_{1,4,0.32}$ have the same entropy jump, but the former has a larger central temperature T^c and larger g-mode frequency.

Table II shows that, as the entropy jump decreases, the damping time of the first g-mode increases dramatically: for $P_{1,5,0.32}$ it is $\tau_{g_1} = 6.27$ s, for $P_{2,3,0.32}$ it is $\tau_{g_1} = 6 \times 10^5$ s. We stress that the quantity we are computing is the *gravitational* damping time, obtained by neglecting all nongravitational dissipative effects. Since the time scale of such effects (viscosity, heat transport, etc.) is of the order of $\tau_{\rm diss} \sim 10$–20 s [26,27], whenever $\tau_{\rm GW} > \tau_{\rm diss}$, the mode is mainly damped by nongravitational dissipative effects.

Since the evaluation of the gravitational damping time is more sensitive to the numerical procedure than that of the mode frequency, we have also computed this quantity by using the approximate formula given in Eq. (23), and indicate its value as $\tau_g^{\rm est}$; we find a reasonable agreement with the data of Table II:

$$\Delta s = 4: \; E_{\rm puls} = 1.047 \text{ km}, \quad L_{\rm GW} = 0.377, \quad \tau_g^{\rm est} = 5.55 \text{ s},$$
$$\Delta s = 1: \; E_{\rm puls} = 0.111 \text{ km}, \quad L_{\rm GW} = 3.8 \times 10^{-6}, \quad \tau_g^{\rm est} = 6 \times 10^4 \text{ s}.$$

Thus, the sharp increase of τ_{g_1} as Δs decreases is due to the sharp decrease of the gravitational luminosity $L_{\rm GW}$ [see Eq. (23)]. As shown in Eq. (25), $L_{\rm GW}$ is (modulo a numerical factor) the squared integral of the function

$$I_{\rm GW} = \nu^3 r^4 \delta\varepsilon^{\ell m}, \tag{42}$$

where ν is the mode frequency and $\delta\varepsilon$ is the perturbed energy density for the considered mode.

In order to understand why $L_{\rm GW}$ decreases so much when the entropy jump decreases, we plot in Fig. 2 $\delta\varepsilon$ (upper panel) and $I_{\rm GW}$ (lower panel) as functions of r, for the stars with profiles $P_{1,5,0.32}$ and $P_{2,3,0.32}$. It is obvious that due to the larger radius of the former configuration and the presence of the factor r^4 in Eq. (25), the emitted power $L_{\rm GW}$ is much larger (indeed the main contribution comes from the envelope), and the damping time is strongly reduced. In addition, the g-mode frequency is also larger in the former configuration, and this contributes further to a larger gravitational wave emission, since $I_{\rm GW} \sim \nu^3$.

Let us now consider the f-modes. For a cold neutron star, the f-mode frequency scales as the average density of the star and the damping time scales as $\tau_f \sim R^4/M^3$. From the data of Table II we see that ν_f increases as the radius decreases (the gravitational mass is nearly the same for all configurations), while the damping time decreases; however, both ν_f and τ_f do not follow quantitatively the cold star scaling laws. The first p-mode frequency has a behavior similar to that of the f-mode, whereas the damping time

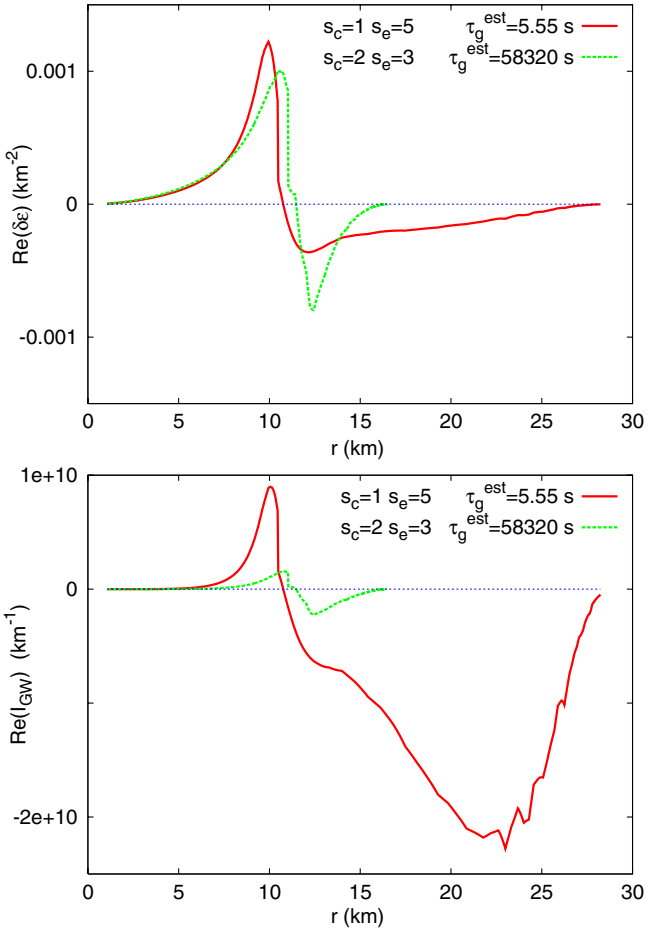

FIG. 2 (color online). Comparison of the perturbed energy density $\delta\varepsilon(r)$, Eq. (26), (upper panel) and of the function $I_{\rm GW}(r)$ given in Eq. (42) (lower panel) for the g-mode of the stellar configurations $P_{1,5,0.32}$ and $P_{2,3,0.32}$. Both functions have been normalized in such a way that the mode pulsation energy is $E_{\rm puls} = 1$ km.

seems to be quite insensitive to changes of the entropy profile.

Finally, we consider a sequence of stellar models with a fixed entropy profile, i.e., $s_c = 1$ in the core and $s_e = 5$ in the envelope, and the lepton fraction varying in the range $Y_e = 0.38, \ldots, 0.28$. The frequency and the damping times of the g_1, f, and p_1-modes are shown in Table III, together with the radius and the gravitational mass of the star. From these data we see that the star radius is a slightly decreasing function of the lepton fraction, and that the behavior of the f and p_1 frequency as a function of the star radius is similar to that described above. Overall, the data show that the dependence of the QNMs eigenfrequencies on the lepton fraction is much weaker than that on the entropy profile.

QNM eigenfrequencies and PNS quasistationary evolution

As mentioned in the Introduction, numerical simulations show that in the early phases of a PNS life the entropy profile has a characteristic evolution which mainly depends on neutrino diffusion processes, and which can be divided in three essential steps:

(1) the entropy per baryon is initially (a few tenths of seconds after bounce) larger in the envelope and lower in the core;
(2) the entropy increases in the core and decreases in the envelope, reaching a roughly uniform profile;
(3) the entropy decreases throughout the star, which eventually becomes a cold neutron star.

The entire process takes about a minute, but we cannot assign precise temporal labels to each step, because they depend on the details of the initial conditions after the bounce and on the dynamical modeling of the evolution, which is beyond the scope of our work (an example of this evolution is shown in Fig. 9 of Ref. [2]).

In this section we construct a sequence of stellar configurations, listed in Table IV, which captures the main qualitative features of a PNS evolution described by steps 1 to 3. Each profile is labeled by a number i, which gives the ordering in time of the simulated evolution. Configurations from $i = 1$ to $i = 4$ (envelope entropy larger than core entropy) refer to the transition from step 1 to step 2, which ends with configuration 5, for which the entropy distribution becomes uniform, but the star is still hot. Then it cools down (configurations 5 to 6) and ends as a zero-temperature NS reaching configuration 7 (step 3). During this "evolution" the lepton number decreases. We have also considered a different sequence, in which the lepton fraction decreases "more rapidly," but the results are very similar to those obtained with the sequence shown in Table IV.

TABLE III. Frequencies (in Hz) and damping times (in s) of the QNMs g_1, f, p_1 for stellar models with baryonic mass $1.5M_\odot$, entropy per baryon in the core $s_c = 1$ and in the envelope $s_e = 5$, and different values of the lepton fraction Y_e. The radius of the star (in km) and its gravitational mass (in solar masses $M_\odot$) are also shown.

Y_e	R	M	ν_{g_1}	τ_{g_1}	ν_f	τ_f	ν_{p_1}	τ_{p_1}
0.38	31.5	1.43	863	6.78	1116	9.75	1415	1.00
0.36	30.6	1.43	883	6.62	1147	6.83	1463	0.89
0.32	29.6	1.42	906	6.25	1194	4.44	1527	0.75
0.30	29.4	1.42	910	5.99	1209	4.01	1543	0.73
0.28	29.4	1.42	908	5.71	1216	3.96	1546	0.72

TABLE IV. Frequencies (in Hz) and damping times (in s) of the QNMs g_1, f, p_1 for a sequence of stellar models which mimic the quasistationary evolution of a PNS with constant baryonic mass $1.5M_\odot$. The star radius (in km) is shown in column 5.

i	s_c	s_e	Y_e	R	ν_{g_1}	τ_{g_1}	ν_f	τ_f	ν_{p_1}	τ_{p_1}
1	1.0	5.0	0.35	30.3	890	6.54	1162	5.89	1484	0.84
2	1.5	4.5	0.32	24.4	910	42.9	1346	0.76	1845	0.55
3	2.0	4.0	0.30	21.3	667	2.3×10^3	1452	0.44	2125	0.73
4	2.0	3.0	0.28	16.4	485	7.6×10^4	1717	0.25	3133	1.80
5	2.0	2.0	0.23	14.1	0	-	1790	0.23	4134	2.59
6	1.0	1.0	$x_\nu = 0$	12.2	0	-	1896	0.21	5879	2.98
7		$T = 0$		11.9	0	-	1898	0.21	6006	3.52

For each configuration we compute the frequencies and damping times of the QNMs g_1, f, p_1. Their values are given in Table IV, and are plotted in Fig. 3 versus the number i which identifies the configuration as explained above. We remark that, as shown in Fig. 3, the gravitational damping time of the g_1-mode sharply increases for $i \gtrsim 2$, while the mode frequency sharply decreases. However, as discussed in Sec. II, as soon as τ_g becomes comparable to $\tau_{\rm diss} \sim 10$–20 s, the mode becomes ineffective with respect to gravitational wave emission, since the stellar oscillations are damped by nongravitational dissipative processes.

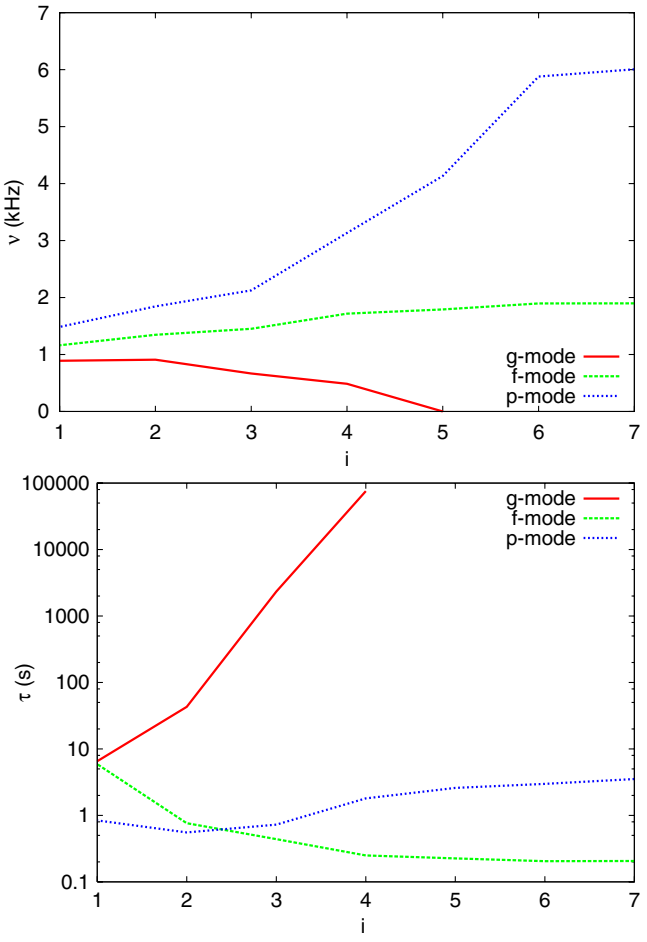

FIG. 3 (color online). Frequencies (upper panel) and damping times (lower panel) of the QNMs g_1, f, p_1 for stellar models corresponding to a possible evolutive sequence of stationary configurations.

The most interesting result which emerges from Table IV and Fig. 3 is that at earlier times, i.e., for $i \leq 2$, the frequencies of the g_1, f, p_1-modes cluster in a small region around 1 kHz, and then tend quite rapidly to the values appropriate for a cold NS (remember that our entire sequence should cover approximately a minute of the PNS evolution). This behavior is similar to that found in [6], where the quasistationary evolution sequence was obtained using a finite-temperature EOS derived within the mean-field approach, treating neutrino transport using the diffusion approximation. The fact that in the very early stages the mode frequency is of the order of 1 kHz (or lower) is important for gravitational wave detection, because the sensitivity of ground-based interferometers LIGO/Virgo decreases quite significantly at larger frequencies.

Another interesting point to note is that during the very early evolution the damping time of all modes is smaller than $\tau_{\rm diss} \sim 10$–20 s. This means that gravitational wave emission is effectively competing in removing energy from the star with dissipation processes related to neutrino viscosity, diffusivity, and thermal conductivity, since typical neutrino time scales are of the order of 10–20 s (see also section 2.1 of [6] for a detailed discussion of this point). At later times, as shown in Fig. 3, the damping time of the g-mode becomes larger than $\tau_{\rm diss}$, and consequently the g-mode will be damped by nongravitational dissipative effects. A more accurate description of the process would require a microscopic modelling of $\tau_{\rm diss}$ during the evolution, which is however beyond the scope of this work.

Furthermore, for $i = 1$ the damping times of the f-mode and g-mode are nearly coincident, showing that in the early stages the g-mode is as effective as the f-mode as a source of gravitational waves. Indeed, the function $I_{\rm GW}$ given by Eq. (42), whose square integral over the star is the gravitational wave luminosity, is similar for the two modes due to a similar profile of the energy density perturbation. At later "times" τ_g becomes much larger than τ_f and, as the PNS tends to the NS final configuration, the g-mode frequency tends to zero.

VI. CONCLUSIONS

In this paper we have investigated how the frequencies and damping times of the quasinormal modes of a proto-neutron star depend on the physical quantities which characterize the stellar configurations during the quasistationary evolution. The most important is the entropy profile inside the star, whereas the dependence on the lepton composition is weaker.

The most interesting result is that if the entropy gradient between core and envelope is large, the frequencies of the first g-mode, of the fundamental mode, and of the first p-mode tend to cluster in a small region near 1 kHz, whereas the damping time of the first g-mode and of the f-mode become comparable. This means that during the initial phases of the quasistationary evolution, when the core entropy is low and the envelope entropy is large, these two modes are competitive as far as gravitational wave emission is concerned.

The damping times are of the order of a few seconds, smaller than dissipative time scales associated to neutrino processes, which are of the order of 10–20 s. Thus, if the star has some mechanical energy to dissipate, it is likely that it will do it through the g_1- and f-modes.

ACKNOWLEDGMENTS

We thank J. A. Pons, K. Glampedakis and D. I. Jones for useful discussions. This work was partially supported by CompStar, a Research Networking Programme of the European Science Foundation, and by the MIUR-PRIN Project No. 2008KRBZTR. L. G. has been partially supported by the FCT Grant No. PTDC/FIS/098025/2008.

APPENDIX A: THE LINDBLOM-DETWEILER EQUATIONS

The system of the Lindblom and Detweiler equations [13,14] consists of four first-order differential equations in the quantities $H_1^{\ell m}(r)$, $K^{\ell m}(r)$, $W^{\ell m}(r)$, $X^{\ell m}(r)$:

$$
\begin{aligned}
H_1^{lm\prime} &= -\frac{1}{r}\left[\ell+1+\frac{2Me^{\lambda}}{r}+4\pi r^2 e^{\lambda}(p-\varepsilon)\right]+\frac{e^{\lambda}}{r}[H_0^{\ell m}+K^{\ell m}-16\pi(\varepsilon+p)V^{\ell m}],\\
K^{\ell m\prime} &= \frac{1}{r}H_0^{\ell m}+\frac{\ell(\ell+1)}{2r}H_1^{\ell m}-\left[\frac{\ell+1}{r}+\frac{\psi'}{2}\right]K^{\ell m}-8\pi(\varepsilon+p)\frac{e^{\lambda/2}}{r}W^{\ell m},\\
W^{\ell m\prime} &= -\frac{\ell+1}{r}W^{\ell m}+re^{\lambda/2}\left[\frac{e^{-\psi/2}}{(\varepsilon+p)c_s^2}X^{\ell m}-\frac{\ell(\ell+1)}{r^2}V^{\ell m}+\frac{1}{2}H_0^{\ell m}+K^{\ell m}\right],\\
X^{\ell m\prime} &= -\frac{\ell}{r}X^{\ell m}+\frac{(\varepsilon+p)e^{\psi/2}}{2}\left[\left(\frac{1}{r}+\frac{\psi'}{2}\right)+\left(r\omega^2e^{-\psi}+\frac{\ell(\ell+1)}{2r}\right)H_1^{\ell m}+\left(\frac{3}{2}\psi'-\frac{1}{r}\right)K^{\ell m}\right.\\
&\quad\left.-\frac{\ell(\ell+1)}{r^2}\psi'V^{\ell m}-\frac{2}{r}\left(4\pi(\varepsilon+p)e^{\lambda/2}+\omega^2e^{\lambda/2-\psi}-\frac{r^2}{2}\left(\frac{e^{-\lambda/2}}{r^2}\psi'\right)'\right)W^{\ell m}\right].
\end{aligned}
\tag{A1}
$$

The remaining perturbation functions, $H_0^{\ell m}(r)$, $V^{\ell m}(r)$, $H_2^{\ell m}(r)$, are given by the algebraic relations

$$
\begin{aligned}
0 &= \left[3M+\frac{(\ell-1)(\ell+2)}{2}r+4\pi r^3p\right]H_0^{\ell m}-8\pi r^3e^{-\psi/2}X^{\ell m}\\
&\quad+\left[\frac{\ell(\ell+1)}{2}(M+4\pi r^3p)-\omega^2r^3e^{-(\lambda+\psi)}\right]H_1^{\ell m}\\
&\quad-\left[\frac{(\ell-1)(\ell+2)}{2}r-\omega^2r^3e^{-\psi}+\frac{e^{\lambda}}{r}(M+4\pi r^3p)(3M-r+4\pi r^3p)\right]K^{\ell m},\\
X^{\ell m} &= \omega^2(\varepsilon+p)e^{-\psi/2}V^{\ell m}-\frac{p'}{r}r^{(\psi-\lambda)/2}W^{\ell m}+\frac{e^{\psi/2}}{2}(\varepsilon+p)H_0^{\ell m},\\
H_0^{\ell m} &= H_2^{\ell m}.
\end{aligned}
\tag{A2}
$$

Equations (A1) and (A2) are solved numerically inside the star, assuming that the perturbation functions are nonsingular near the center. An asymptotic expansion of the equations near $r=0$ shows that this requirement implies

$$X^{\ell m}(0) = [\varepsilon(0) + p(0)]e^{\psi(0)/2}\left[\left(\frac{4\pi}{3}[\varepsilon(0) + 3p(0)] - \omega^2\frac{e^{-\psi(0)}}{\ell}\right)W^{\ell m}(0) + \frac{1}{2}K^{\ell m}(0)\right],$$

$$H_1^{\ell m}(0) = \frac{1}{\ell(\ell+1)}[2\ell K^{\ell m}(0) + 16\pi[\varepsilon(0) + p(0)]W^{\ell m}(0)]. \tag{A3}$$

On the stellar surface, $r = R$, one assumes continuity of the perturbation functions and the vanishing of the Lagrangian pressure perturbation, i.e.,

$$X^{\ell m}(R) = 0. \tag{A4}$$

In the exterior, the metric perturbations are described by the Zerilli function

$$Z^{\ell m} = \frac{r^{\ell+2}}{nr + 3M}(K^{\ell m} - e^{\psi}H_1^{\ell m}), \tag{A5}$$

[where $n = (\ell - 1)(\ell + 2)/2$], which is solution of the Zerilli equation

$$\frac{d^2Z^{\ell m}}{dr_*^2} + [\omega^2 - V_Z(r)]Z^{\ell m} = 0 \tag{A6}$$

with $r_* \equiv r + 2M\ln(r/2M - 1)$ and

$$V_Z \equiv e^{-\lambda}\frac{2n^2(n+1)r^3 + 6n^2Mr^2 + 18nM^2r + 18M^3}{r^3(nr + 3M)^2}. \tag{A7}$$

Finally, to describe free oscillations of the star we must impose the outgoing wave boundary condition

$$Z^{\ell m}(r) \to e^{-i\omega r_*} \qquad (r \to \infty). \tag{A8}$$

A solution of Eqs. (A1) and (A6) satisfying the boundary conditions (A3), (A4), and (A8) only exists for a discrete set of (complex) values of the frequency $\omega = 2\pi\nu + i/\tau$: the quasinormal modes of the star.

[1] C. D. Ott, Classical Quantum Gravity **26**, 063001 (2009).
[2] J. A. Pons, S. Reddy, M. Prakash, J. M. Lattimer, and J. A. Miralles, Astrophys. J. **513**, 780 (1999).
[3] J. A. Pons, J. A. Miralles, M. Prakash, and J. M. Lattimer, Astrophys. J. **553**, 382 (2001).
[4] J. A. Pons, A. W. Steiner, M. Prakash, and J. M. Lattimer, Phys. Rev. Lett. **86**, 5223 (2001).
[5] T. Fisher, S. C. Whitehouse, A. Mezzacappa, F.-K. Thielemann, and M. Liebendörfer, Astron. Astrophys. **517**, A80 (2010).
[6] V. Ferrari, G. Miniutti, and J. A. Pons, Mon. Not. R. Astron. Soc. **342**, 629 (2003).
[7] V. Ferrari, G. Miniutti, and J. A. Pons, Classical Quantum Gravity **20**, S841 (2003).
[8] N. Andersson, V. Ferrari, D. I. Jones, K. D. Kokkotas, B. Krishnan, J. Read, L. Rezzolla, and B. Zink, Gen. Relativ. Gravit. **43**, 409 (2011).
[9] Y. Kojima, Phys. Rev. D **46**, 4289 (1992).
[10] V. Ferrari, L. Gualtieri, and S. Marassi, Phys. Rev. D **76**, 104033 (2007).
[11] E. Gaertig and K. D. Kokkotas, Phys. Rev. D **78**, 064063 (2008).
[12] K. S. Thorne and A. Campolattaro, Astrophys. J. **149**, 591 (1967).
[13] L. Lindblom and S. L. Detweiler, Astrophys. J. Suppl. Ser. **53**, 73 (1983).
[14] S. L. Detweiler and L. Lindblom, Astrophys. J. **292**, 12 (1985).
[15] S. Chandrasekhar and V. Ferrari, Proc. R. Soc. A **432**, 247 (1991).
[16] J. P. Cox, *Theory of Stellar Pulsation* (Princeton University Press, Princeton 1980).
[17] S. Chandrasekhar and V. Ferrari, Proc. R. Soc. A **434**, 449 (1991); K. D. Kokkotas and B. F. Schutz, Mon. Not. R. Astron. Soc. **255**, 119 (1992).
[18] D. W. Meltzer and K. S. Thorne, Astrophys. J. **145**, 514 (1966).
[19] P. Haensel, K. P. Levenfish, and D. G. Yakovlev, Astron. Astrophys. **394**, 213 (2002).
[20] N. Andersson and K. D. Kokkotas, Mon. Not. R. Astron. Soc. **299**, 1059 (1998).
[21] O. Benhar, V. Ferrari, and L. Gualtieri, Phys. Rev. D **70**, 124015 (2004).
[22] V. Ferrari, Bulletin of the Astronomical Society of India **39**, 203 (2011), http://www.ncra.tifr.res.in/~basi/11March/203392011.pdf.
[23] K. S. Thorne, Astrophys. J. **144**, 201 (1966).
[24] P. N. McDermott, H. M. Van Horn, and J. F. Scholl, Astrophys. J. **268**, 837 (1983).
[25] M. Tassoul, Astrophys. J. Suppl. Ser. **43**, 469 (1980).
[26] B. T. Goodwin and C. J. Pethick, Astrophys. J. **253**, 816 (1982).
[27] L. J. van den Horn and C. H. van Weert, Astron. Astrophys. **136**, 74 (1984), http://articles.adsabs.harvard.edu/cgi-bin/nph-iarticle_query?1984A%26A...136...74V&data_type=PDF_HIGH&whole_paper=YES&type=PRINTER&filetype=.pdf.
[28] K. S. Thorne, Astrophys. J. **158**, 1 (1969).
[29] M. Baldo, *Nuclear Methods and the Nuclear Equation of State*, International Review of Nuclear Physics Vol. 8 (World Scientific, Singapore, 1999).
[30] C. Bloch and C. De Dominicis, Nucl. Phys. **7**, 459 (1958); **10**, 181 (1959).
[31] M. Baldo and L. S. Ferreira, Phys. Rev. C **59**, 682 (1999).
[32] J. Carlson, V. R. Pandharipande, and R. B. Wiringa, Nucl. Phys. **A401**, 59 (1983); R. Schiavilla, V. R. Pandharipande, and R. B. Wiringa, Nucl. Phys. **A449**, 219 (1986); B. S. Pudliner, V. R. Pandharipande, J. Carlson, S. C. Pieper, and R. B. Wiringa, Phys. Rev. C **56**, 1720 (1997).

[33] M. Baldo, I. Bombaci, and G. F. Burgio, Astron. Astrophys. **328**, 274 (1997), http://articles.adsabs.harvard.edu/cgi-bin/nph-iarticle_query?1997A%26A...328..274B&data_type=PDF_HIGH&whole_paper=YES&type=PRINTER&filetype=.pdf.

[34] X. R. Zhou, G. F. Burgio, U. Lombardo, H.-J. Schulze, and W. Zuo, Phys. Rev. C **69**, 018801 (2004).

[35] Z. H. Li and H.-J. Schulze, Phys. Rev. C **78**, 028801 (2008).

[36] R. B. Wiringa, V. G. J. Stoks, and R. Schiavilla, Phys. Rev. C **51**, 38 (1995).

[37] O. E. Nicotra, M. Baldo, G. F. Burgio, and H.-J. Schulze, Astron. Astrophys. **451**, 213 (2006); O. E. Nicotra, M. Baldo, G. F. Burgio, and H.-J. Schulze, Phys. Rev. D **74**, 123001 (2006).

[38] G. F. Burgio and H.-J. Schulze, Phys. At. Nucl. **72**, 1197 (2009).

[39] G. F. Burgio and H.-J. Schulze, Astron. Astrophys. **518**, A17 (2010).

[40] G. F. Burgio, H.-J. Schulze, and A. Li, Phys. Rev. C **83**, 025804 (2011).

[41] H. Shen, H. Toki, K. Oyamatsu, and K. Sumiyoshi, Nucl. Phys. **A637**, 435 (1998); Prog. Theor. Phys. **100**, 1013 (1998); http://user.numazu-ct.ac.jp/~sumi/eos/index.html.

[42] D. Gondek, P. Haensel, and J. L. Zdunik, Astron. Astrophys. **325**, 217 (1997), http://articles.adsabs.harvard.edu/cgi-bin/nph-iarticle_query?1997A%26A...325..217G&data_type=PDF_HIGH&whole_paper=YES&type=PRINTER&filetype=.pdf.

[43] K. Strobel, C. Schaab, and M. K. Weigel, Astron. Astrophys. **350**, 497 (1999), http://articles.adsabs.harvard.edu/cgi-bin/nph-iarticle_query?1999A%26A...350..497S&data_type=PDF_HIGH&whole_paper=YES&type=PRINTER&filetype=.pdf.

[44] T. Fischer, S. C. Whitehouse, A. Mezzacappa, F.-K. Thielemann, and M. Liebendörfer, Astron. Astrophys. **499**, 1 (2009).

[45] P. N. McDermott, H. M. van Horn, and C. J. Hansen, Astrophys. J. **325**, 725 (1988).